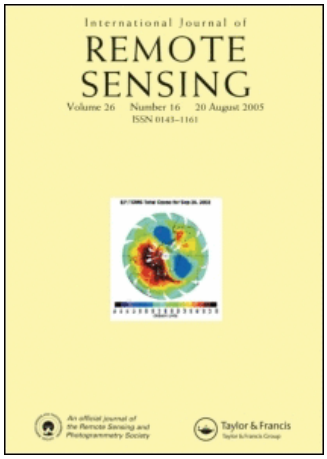

International Journal of Remote Sensing
Publication details, including instructions for authors and subscription information:
http://www.informaworld.com/smpp/title~content=t713722504

Absolute calibration of AVHRR visible and near-infrared channels using ocean and cloud views

E. Vermote [a]; Y. J. Kaufman [b]
[a] Laboratory for Global Remote Sensing, Lefrak Hall, University of Maryland, College Park, Maryland, U.S.A.
[b] NASA/GSFC, Laboratory for Atmospheres Code 913, Greenbelt, MD, U.S.A.

Online Publication Date: 10 September 1995
To cite this Article: Vermote, E. and Kaufman, Y. J. (1995) 'Absolute calibration of AVHRR visible and near-infrared channels using ocean and cloud views', International Journal of Remote Sensing, 16:13, 2317 - 2340
To link to this article: DOI: 10.1080/01431169508954561
URL: http://dx.doi.org/10.1080/01431169508954561

INT. J. REMOTE SENSING, 1995, VOL. 16, NO. 13, 2317–2340

Absolute calibration of AVHRR visible and near-infrared channels using ocean and cloud views

E. VERMOTE

Laboratory for Global Remote Sensing, Lefrak Hall, University of Maryland, College Park Maryland, U.S.A.

and Y. J. KAUFMAN

Laboratory for Atmospheres Code 913, NASA/GSFC, Greenbelt MD 20771, U.S.A.

(Received 8 February 1994; in final form 21 August 1994)

Abstract. Methods for absolute calibration of visible and near-infrared sensors using ocean and cloud views have been developed and applied to channels 1 (red) and 2 (near-infrared) of the Advanced Very High Resolution Radiometer (AVHRR) for the NOAA-7, -9 and -11 satellites. The approach includes two steps. First step is intercalibration between channels 1 and 2 using high altitude (12 km and above) bright clouds as 'white' targets. This cloud intercalibration is compared with intercalibration using ocean glint. The second step is an absolute calibration of channel 1 employing ocean off-nadir view (40–70°) in channels 1 and 2 and correction for the aerosol effect. In this process the satellite measurements in channel 2, corrected for water vapour absorption are used to correct channel 1 for aerosol effect. The net signal in channel 1 composed from the predictable Rayleigh scattering component is used to calibrate this channel. The result is an absolute calibration of the two AVHRR channels. NOAA-9 channels 1 and 2 show a degradation rate of 8·8 per cent and 6 per cent, respectively, during 1985–1988 and no further degradation during 1988–1989 period. NOAA-11 shows no degradation during the 1989 mid 1991 period. This trend is similar to the calibration trend obtained using desert site observations, the absolute calibration found in this work for both sensors is lower by 17 to 20 per cent (suggesting higher degradation) from the absolute calibration of Abel *et al.* (1993, *Journal of Atmospheric and Ocean Technology*, **10**, 493–508), that used aircraft measurements. Furthermore we show that application of the calibration of Abel *et al.* or the present one for remote sensing of aerosol over Tasmania, Australia failed to predict correctly the aerosol optical thickness measured there. The only way to reconcile all these differences is by allowing for a shift of 17 nm towards longer wavelengths of the AVHRR channel 1 effective wavelength. We show that with this shift, we get an agreement between the two absolute calibration techniques (±3 per cent), and both of them do predict correctly the optical thickness in the two channels (±0·02). Recent work in preparation for publication (Vermote *et al.*, 1995, in preparation) indicates that this shift is due to an out of band transmission (6 per cent at 900 nm) for AVHRR channel 1 previously unidentified.

1. Introduction

Quantitative applications of Advanced Very High Resolution Radiometer (AVHRR) data on board the National Oceanographic and Atmospheric Administration (NOAA) satellites for remote sensing of vegetation dynamics (Justice *et al.*

1985, Tucker and Sellers 1985, Holben 1986), transport of pollution and smoke aerosol particles (Kaufman *et al.* 1990, Holben *et al.* 1992) and radiative properties of clouds (Arking and Childs 1985, Coakley *et al.* 1987, Kaufman and Nakajima 1993) require accurate radiometric calibration. The AVHRR does not have any on board calibration capability for the visible and near-infrared channels. Its design and launch environment was not structured to maintain stable calibration (Mekler and Kaufman 1995). As a result, calibration of the AVHRR has been an area of growing concern in the scientific community for the past few years. Several methods for both relative and absolute in-flight calibrations have been developed. The methods for relative calibration use AVHRR observations of surface targets with stable though unknown reflectivity, monitoring the change of the calibration as a function of time and transferring it from one AVHRR sensor to another (Holben *et al.* 1990, Staylor 1990, Rao *et al.* 1993).

Methods for absolute calibration are based on AVHRR measurements of radiances above a surface target (land or water) and simultaneous measurements of the combined surface and atmospheric reflectance from high flying aircraft (Smith *et al.* 1988, Abel *et al.* 1993) or measurements of the surface reflectance and the atmospheric optical properties (Koepke 1982, Frouin and Gautier 1987, Teillet *et al.* 1990, Mitchell *et al.* 1992). Even though the pre-flight calibration was well documented (Price 1987, 1988), possible changes in the calibration during the long storage before launch and due to the trauma during the launch (Mekler and Kaufman 1995) require detailed absolute calibration during the flight. Since these absolute calibrations require aircraft operations or field measurements, they are expensive and cannot be performed on a frequent basis. Calibrations over the land using simultaneous measurements of the surface reflectance from the AVHRR and from aircraft or surface-based observations are affected by uncertainties in the calibration of the instruments that are used to calibrate the satellite sensor. The registration of the surface targets that are observed simultaneously by the satellite and the aircraft or field instruments is difficult and causes uncertainties (Abel *et al.* 1993). Differences in the view direction and uncertainty in the surface bidirectional reflectance can cause additional errors.

An alternative approach for absolute calibration, that does not require aircraft or field measurements, was developed by Fraser and Kaufman (1986) for the Visible Infrared Spin Scan Radiometer (VISSR) carried on the geostationary satellites GOES-5 and -6. This approach is based on the large contribution of molecular scattering over the ocean to the radiance detected by the satellite for slant view directions. For the effective wavelength of the VISSR of 0·61 μm, molecular scattering contributes to 80 per cent of the signal. The rest of the radiance is due to aerosol scattering, glint reflection of sky light, underwater reflectance and attenuation by ozone absorption. These perturbations in the radiance were estimated using climatology. The method clearly showed the instability of the manually tuned gains of GOES-5 and the stability of the calibration of GOES-6 that was found to be very close to the pre-flight values. Kaufman and Holben (1993) applied this method in a similar fashion to the AVHRR band 1 with an effective wavelength of 0·63 μm. The results were not as clearly successful as for the GOES calibration. The lower molecular scattering for the slightly higher wavelength and the smaller number of measurements used for large view directions resulted in larger dependence on the uncertainty in the aerosol optical thickness and larger noise in the calibration. Small variations in the aerosol optical thickness of $\Delta\tau_a = \pm 0{\cdot}05$ can cause a 10 per cent

error in the calibration. In this paper, the calibration technique for the AVHRR using radiances over the simultaneous use of AVHRR channels 1 and 2 over the ocean and over high bright clouds to derive the AVHRR calibration of channels 1 and 2 simultaneously with the determination of the aerosol loading. High, bright clouds over the oceans are introduced as a spectrally neutral reflector to intercalibrate channels 1 and 2, one relative to the other. The effect of water vapour absorption in channel 2 is calculated using the split window technique to estimate total precipitable water vapour (Dalu 1986). We will show in this paper that this combined technique reduces the uncertainty due to the presence of aerosol and due to variations in the rough ocean reflection introduced by a varying wind speed. The combined analysis of visible and near-infrared channels for the calibration of a satellite sensor was first applied by Vermote *et al.* (1992) for the calibration of the Systeme Pour l'Observation de la Terre (SPOT) Haute Resolution Visible (HRV) radiometer. They found that the calibration derived using the ocean method agreed with the official CNES in-flight calibration within 2 per cent.

The calibration technique is explained in the next section. The accuracy of the present method is examined. The method is applied to NOAA-7, -9 and -11 AVHRR data from 1981 to 1992. The results of calibration are compared to previously published values for the NOAA-9 and -11 AVHRR.

2. The calibration methods

2.1. *Definitions*

Calibration coefficients convert satellite measured signal to radiance units ($Wm^{-2}sr^{-1}\mu m^{-1}$). It is convenient to discuss it with radiances expressed in reflectance units, L^*:

$$L^* = \frac{\pi L d^2}{E_0} \tag{1}$$

where L is the radiance [$Wm^{-2}str^{-1}\mu m^{-1}$], d is the Sun-Earth distance in astronomical units and E_0 is the exo-atmospheric solar irradiance [$Wm^{-2}\mu m^{-1}$] integrated over the channel response. In this case, calibration is expressed as the relation between the signal and the reflection (see Kaufman and Holben 1993 for details). The reflectance, ρ, is computed from the normalized radiance, L^*, by:

$$\rho = L^*/\mu_S \tag{2}$$

where μ_s is the cosine of the solar zenith angle.

2.2. *Intercalibration between channels 1 and 2*

Because the cloud drop size is typically an order of magnitude larger than the wavelength of the AVHRR channels 1 and 2, the reflective properties of cloud drops in the 0·6–1·0μm window are spectrally neutral. Differences between the apparent cloud reflectance in AVHRR channels 1 and 2 can be due to differences in water vapour and ozone absorption, aerosol and molecular scattering and underlying surface reflectance. To minimize these differences the intercalibration technique is based on high, reflective clouds over the ocean. For these clouds the spectral effect of aerosol scattering and water vapour absorption is very small.

2.2.1. *Description*

Clouds observed close to nadir ($\pm 10°$) are considered a lambertian reflector. We use clouds that are thick enough so that the radiative effect of the atmosphere and

surface below the cloud can be neglected. Therefore, the signal at the top of the atmosphere, $\rho(z)$, can be written as a function of the cloud top altitude z:

$$\rho(z) = Tg(z)\left[\rho_z(z) + T_a(z)\frac{\rho\text{cloud}}{1 - S(z)\rho_{\text{cloud}}}\right] \tag{3}$$

where $T_g(z)$ is the gaseous transmission above the cloud, $\rho_a(z)$ is the intrinsic reflectance of the atmosphere above the cloud, $T_a(z)$ is the transmission due to scattering of the atmosphere above the cloud, and $S(z)$ is the albedo of the atmosphere above the cloud.

If the cloud is high enough (above 12 km), then the aerosol and water vapour have a negligible influence on the signal because they are located mainly in the lower layers of the atmosphere. The only contributions to the observed signal are from the cloud reflectance, molecular scattering, and absorption by oxygen and ozone. Therefore, the apparent reflectance observed by the satellite above the cloud can be written for both channels 1 and 2 of the AVHRR as:

$$\rho^i_{(z)} = T^i_{\text{goz}}\left[T^i_{\text{gox}}(z/2)\rho^i_r(z) + T^i_{\text{gox}}(z)T^i_r(z)\frac{\rho_c}{(1 - S^i_r(z)\rho_c)}\right] \qquad i = 1,2 \tag{4}$$

T_{goz} represents the gaseous transmission due to ozone layer (above 20 km). T_{gox} represents the gaseous transmission due to oxygen. It affects the cloud reflectance and the molecular absorption differently because most oxygen absorption is above the cloud but is mixed with the molecular scattering. In order to simplify the rest of the paper we will ignore this effect in the following equations even though computations are performed considering this coupling. $\rho_r(z)$ is the Rayleigh reflectance due to molecules located above z. $T_r(z)$ is the moledular scattering transmission. ρ_c is the cloud reflectance. $S_r(z)$ is the molecules layer albedo.

The actual reflectance computed from the AVHRR measured radiance is lower due to gain degradation (r_i). It is given by (4) and the simplification for T_{gox}:

$$\rho^m_i = \rho_i r_i = T^i_{\text{goz}} T^i_{\text{gox}}(z)\left[\rho^i_r(z) + T^i_r(z)\frac{\rho_c}{(1 - S^i_r(z)\rho_c)}\right] r_i, \qquad i = 1,2 \tag{5}$$

where ρ^m_i are apparent reflectances obtained from the measured AVHRR signals using the pre-flight calibration for channels 1 and 2 (Price 1987, 1988) and r_i are the respective degradation coefficients (e.g., Kaufman and Holben 1993, Rao *et al.* 1993) for channel i ($i = 1,2$).

In order to relate the AVHRR measurements directly to the cloud reflectance, the measurements have to be corrected for the atmospheric scattering and absorption. Assuming that the Rayleigh scattering is small relative to the cloud reflectance and therefore neglecting the effect of calibration degradation on ρ_r, the corrected AVHRR measurements ρ' in the two channels are:

$$\rho'_i = \frac{\dfrac{\rho^m_i}{T^i_{\text{goz}} T^i_{\text{gox}}(z)} - \rho^i_r(z)}{T^i_r(z)} \cong \frac{r_i \rho_c}{1 - S^i_r(z)\rho_c} \tag{6}$$

Then correcting also for the atmospheric albedo, $S^r(z)$, it is found that:

$$\rho''_i = \frac{\rho'_i}{1 + S^r_i(z)\rho'_i} = r_i \rho_c \tag{7}$$

ρ_i'' is directly related to the cloud reflectance ρ_c through the degradation in the calibration of r_i. Assuming that the reflectance of the cloud itself is not dependent on the wavelength in the range from 0·60 to 1·0 μm, we get:

$$\rho_1''/\rho_2'' = r_1/r_2 = r_{12} \tag{8}$$

2.2.2. *Error budget*

Lambertian clouds. Cloud observations were conducted for view zenith angles between 0 and 10° in order to minimize gaseous absorption and scattering. Furthermore, because the ratio of cloud reflectances in two spectral channels is utilized in this method, any remaining errors due to non-lambertianity are expected to cancel out.

Aerosol and water vapour. Pixels of clouds were chosen over the Pacific Ocean based on the apparent cloud top temperature in channel 4 (10·8 μm) being in the range from 220 to 225 K at tropical latitudes where most of these high convective clouds can be found. This corresponds to an altitude range from 12 to 13 km, which is well above most water vapour or aerosol layers. Figure 1 shows the dependence on temperature in channel 4 of the apparent reflectance of clouds for both channels. Both channel 1 and 2 signals increase with reduction of cloud top temperature, due to the presence of thicker and more developed clouds and due to the decreasing amount of water vapour absorption. Figure 2 shows the reflectance ratio, ρ_1/ρ_2, versus temperature. The reduction in the ratio with decreasing temperature is due to the lower water vapour concentration and absorption. The clouds selected to determine the calibration ratio r_{12} are located at the lower end of the temperature range, where the water vapour effect is minimal and therefore the reflection ratio

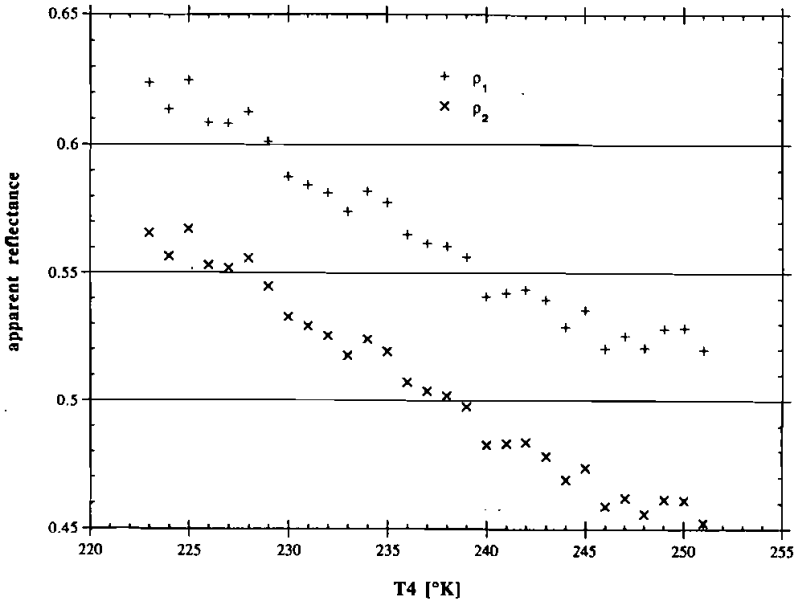

Figure 1. Cloud reflectances observed in channel 1, ρ_1 (0·63 μm), and 2, ρ_2 (0·83 μm) of AVHRR as a function of the cloud top temperature based on channel 4.

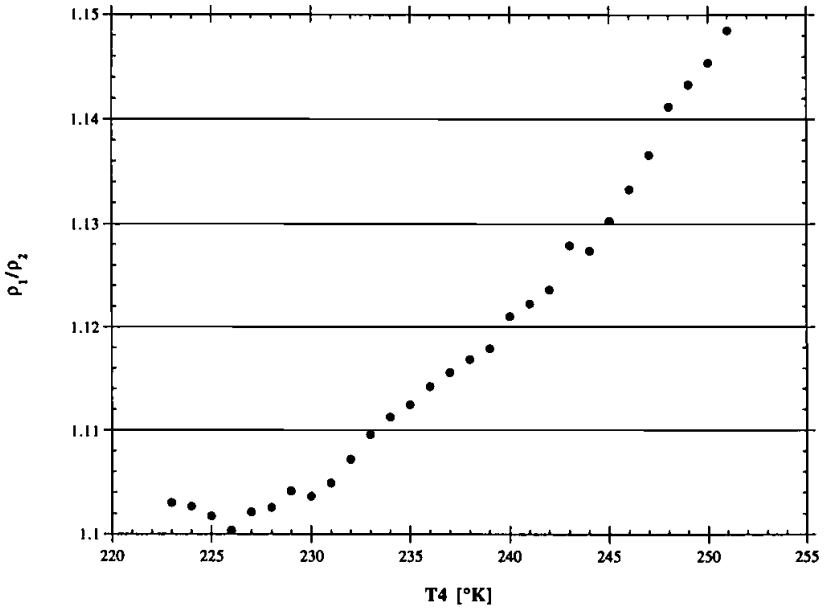

Figure 2. The ratio of observed cloud reflectances ρ_1/ρ_2 as function of the temperature in channel 4.

reaches a plateau. We found out that the residual amount of water vapour, for a tropical profile, at this range of altitudes is of the order of $0{\cdot}002\,g\,cm^{-2}$, which corresponds to transmission of 0·999. Thus, the uncertainty due to neglect of water vapour absorption inside and above clouds is negligible in this altitude range.

Rayleigh correction. For clouds of apparent reflectance greater than 0·5 and altitude higher than 12 km, and for a view zenith angle less than 10°, the terms ρ_r, T_r and S_r only influence 1 per cent of the total signal. Therefore, ignoring the effect of degradation of calibration on these terms will lead to a maximal error of 0·3 per cent, for a degradation of calibration of 30 per cent.

Ozone and oxygen correction. The oxygen absorption is weak in both channels and depends mainly on altitude. The uncertainty in the altitude is of the order of 1 km, therefore the uncertainty in total oxygen amount is less than 5 per cent. The variation of the transmission in both channels due to the variation of oxygen amount is negligible.

The stratospheric ozone amount is taken to be constant and equal to 240 Dobson units. This value is based on a climatology derived from Stratospheric Aerosol and Gas Experiment (SAGE) observations (Fishman *et al.* 1990) and on the selection of only high clouds at tropical latitudes (−25 to +25°) and over the Pacific Ocean (longitude between −135 and 175°). The relative variation of the ozone amount should be of the order of 20 Dobson units. That translates for an airmass of 2 to an uncertainty of 1 per cent in the radiance for channel 1 and similar uncertainty in r_{12}.

Total error. If we sum the squares of all the error sources investigated (table 1) and then take the square root, the overall uncertainty of the method is about 2 per cent.

Therefore the absolute intercalibration of channel 1 relative to channel 2 is defined with an uncertainty of ± 2 per cent. There could be other sources of error that have not been considered such as stratospheric aerosol effects, but we can avoid significant concentrations by using locations and times with small stratospheric loading based on aerosol monitoring data sets such as the SAGE data (McCormick and Veiga 1992) or the NOAA weekly composite (Stowe *et al.* 1992). The analysis of long-term continuous datasets, as we will demonstrate in the next section, will be used to verify the error budget, since the error sources vary on a much higher frequency than sensor deterioration.

2.3. *Rayleigh calibration for channel 1*

The simulations are performed with a radiative transfer code based on the Successive Order of Scattering (SOS) method to simulate the scattering effect of molecules and aerosols taking into account as ground boundary condition both a lambertian contribution for a clear water case and a wind disturbed sea surface according to the Cox and Munk model (1965). The SOS model accounts for a mixing of Rayleigh and aerosol scattering by dividing the atmosphere into 27 layers. The model has been validated and published by Deuzé *et al.* (1989). Theoretical calculations of the radiance in both AVHRR channels are done assuming a clear water chlorophyll content for oceanic conditions of $0{\cdot}3\,\mathrm{mg\,m^{-3}}$ (Morel 1988), for a wind speed of $10\,\mathrm{m\,s^{-1}}$, for several water vapour values, and an aerosol model representative of maritime-aerosol particle distribution with a scale height of 2 km with optical thickness of 0·10 at 0·55 μm.

The absorption effect of ozone and oxygen was computed using an explicit formulation fitted from 5S model runs (Tanré *et al.* 1990) and multiplying the SOS reflectance by the transmission computed.

The water vapour absorption effect was taken into account in the successive order of scattering code in a way similar to the approach adopted by Fraser *et al.* (1992) assuming a scale height of 3 km for water vapour. The computations of the signal were performed at one effective wavelength for channel 1 and two wavelengths for channel 2 to account better for coupling between water vapour absorption and scattering. Because of the relative high absorption present in channel 2, this channel was divided into two parts (0·7000–0·890 μm small absorption, 0·890–1·100 μm high absorption) to account accurately for the aerosol-water vapour

Table 1. Error budget for the intercalibration of channel 1 versus channel 2 of AVHRR using oceanic clouds.

Error source	Uncertainty	$\delta r_{12}/r_{12}$
Non-lambertianity effect in θ_s	Unknown	0%
Tropospheric aerosol above 12 km	0%	0%
Water vapour above 12 km	0·002 cm	<0·01%
Molecules effect correction	30%	0·3%
Oxygen amount	5%	<0·01%
Ozone amount	20 Dobson units	1%
Whiteness of cloud	1%	1%
Total (r.m.s.)		1·5%

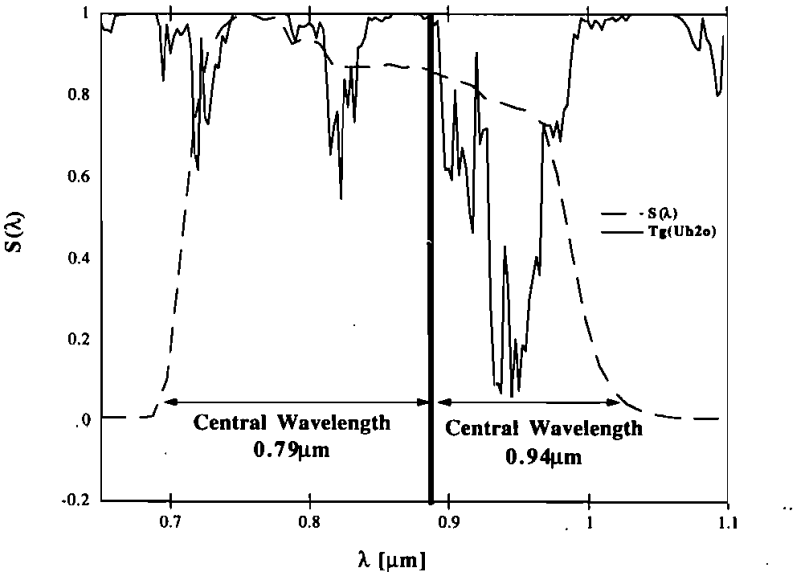

Figure 3. Definition of the two bands used to compute the signal in AVHRR channel 2. For the atmospheric model selected, band 1 (0·6–0·89 μm) represents 75 per cent of the signal, band 2 (0·89–1·12 μm) represents 25 per cent of the signal.

coupling (see figure 3). Table 2 summarized, for each of the bands, the parameters used in the SOS runs as well as the formula for gaseous transmission.

2.3.1. *Description*

For a cloudless air mass over the ocean with a small amount of haze and far from sun glint, the major contribution to the upward radiance in the visible part of

Table 2. Parameters used in the computation of the signal over the ocean. For the computation of water vapour transmission (last line), M represents the air mass and U_{H_2O} the water vapour integrated content (g cm^{-2}).

		Channel 2 = 0·75 band 1 + 0·25 band 2	
	Channel 1	Band 1	Band 2
Central wavelength	0·63 μm	0·79 μm	0·94 μm
Rayleigh optical depth	0·058	0·01118	0·02334
Aerosol optical depth	0·0998	0·0970	0·0930
Aerosol model		Haze M	
		$\frac{dN(r)}{dr} = re^{-(8\cdot9443\sqrt{r})}$	
		refraction index $n = 1\cdot33 + 0\cdot0i$	
Lambertian reflectance (water + foam)	0·0045	0·0020	0·0020
Directional reflectance	Cox and Munk's (1965) model, wind speed = 10 m s^{-1}		
$T_g(H_2O) = \exp - (a(M \cdot U_{H_2O})^b)^2$	$a = 0\cdot0105$	$a = 0\cdot0254$	$a = 0\cdot2041$
	$b = 0\cdot6705$	$b = 0\cdot5886$	$b = 0\cdot5382$

the spectrum is from molecular scattering (70–80 per cent—Kaufman and Holben 1993), which can be accurately computed using a radiative transfer model. The remaining contribution (20–30 per cent) is mainly due to aerosol scattering. Using information from channels 1 and 2 simultaneously (once the two channels are intercalibrated), we shall show that the absolute calibration of channel 1 and aerosol loading can be simultaneously derived from the AVHRR measurements. An aerosol model has to be assumed, in this case a maritime model. This is similar to the approach used to calibrate the SPOT/HRV sensor (Vermote *et al.* 1992).

The degradation calibration coefficient r_1 is defined by

$$r_1 = \frac{\rho_1^m}{\rho_1^r} \tag{9}$$

where ρ_1^m is the reflectance deduced from the sensor measurements using the pre-flight calibration and ρ_1^r is the *true* reflectance.

The unknown aerosol concentration and wind speed are dealt with using a baseline model (aerosol optical thickness of 0·10, wind speed of $10\,\mathrm{m\,s^{-1}}$) for the reflectance in channels 1 and 2, ρ_1^t and ρ_2^t, and a perturbation to it, $\delta\rho_1$ and $\delta\rho_2$. The 'true' reflectance ρ_1^r is described by a base model (ρ_1^t) and a perturbation $\delta\rho_1$ that accounts for the difference in the atmospheric conditions from the base model:

$$\rho_1^r = \rho_1^t + \delta\rho_1 \tag{10}$$

The reflectance derived from the satellite data using pre-flight calibration is (equations (9) and (10))

$$\rho_1^m = r_1\rho_1^t + r_1\delta\rho_1 \tag{11}$$

A similar relationship holds for the observed reflectance in channel 2:

$$\rho_1^m = r_2\rho_2^t + r_2\delta\rho_2 \tag{12}$$

For a maritime aerosol model, the relationship between $\delta\rho_1$ and $\delta\rho_2$ is defined by the spectral dependence of this perturbation I_{12}:

$$\delta\rho_1 = I_{12}\delta\rho_2 \tag{13a}$$

where I_{12} is derived from simulations of the signal for both channels 1 and 2 with aerosol optical thickness of 0·15 and 0·05, respectively. In extenso, I_{12} is computed as:

$$I_{12} = \frac{\rho_1(\tau_a = 0{\cdot}015) - \rho_1(\tau_a = 0{\cdot}05)}{\rho_2(\tau_a = 0{\cdot}015) - \rho_2(\tau_a = 0{\cdot}05)} \tag{13b}$$

Note that I_{12} is almost independent of the unknown parameters, e.g., wind speed and optical thickness.

(11)–(13) can be solved for ρ_1^m:

$$\rho_1^m = r_1\rho_1^t + r_1 I_{12}(\rho_2^m - r_2\rho_2^t)/r_2 \tag{14}$$

Solving for r_1 and using $r_{12} = r_1/r_2$, it is found that:

$$r_1 = \frac{\rho_1^m - r_{12}I_{12}\rho_2^m}{\rho_1^t - I_{12}\rho_2^t} \tag{15}$$

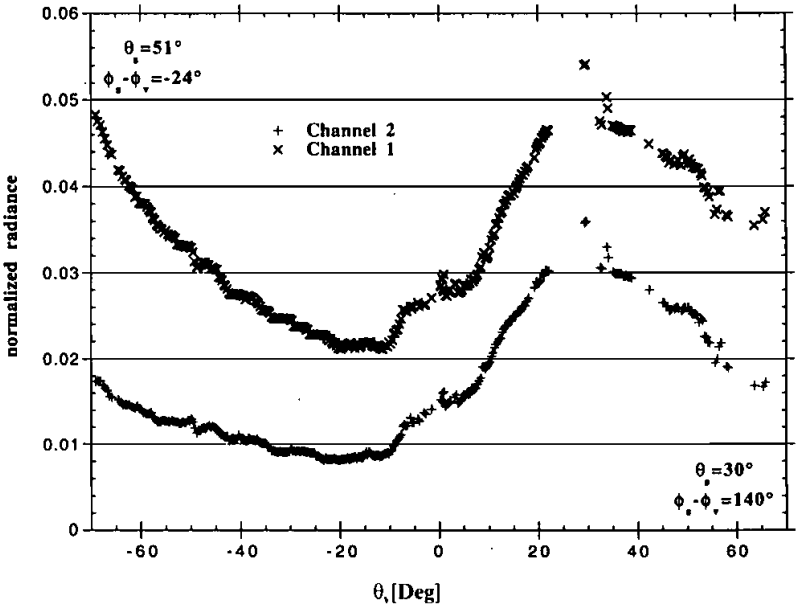

Figure 4. The radiances observed in channels 1 and 2 of AVHRR over ocean as a function of the view angle θ_v, negative values of the view angle refer to backscattering direction. Note the higher glint reflectance for $\theta_v = \theta_s$.

where r_{12} is the intercalibration coefficient computed with the method previously outlined.

In practice, the calculation of r_1 is based on a number of measurements. The data sets are extracted from data taken over the Pacific Ocean where for a period of 9 days, a rigorous cloud screening is performed (Stowe *et al.* 1991) and a composite of the non-cloudy pixels and no-cloud-shadowed pixels is produced using the minimum value in channel 1. The result of this 'geometrical composite' is then screened manually to select a zone of 25 scan lines where the cloud amount is low and the Rayleigh contribution significant. To maximize Rayleigh scattering, data were chosen as close as possible to the principal plane, where in the backscattering direction the Rayleigh phase function reaches a maximum. An average of the radiances is then taken for each view direction for both channels. After subtracting the deep-space count (Holben *et al.* 1990) the values were converted to reflectance units using the pre-flight calibration coefficients. For each pixel of the anti-specular portion of the scan (angle of view 40–70°, see figure 4) the numerator of (13) is plotted versus the denominator of (13) (figure 5). The water vapour amount is determined from the split window technique as detailed in Vermote *et al.* (1993) based on Dalu (1986). The slope of the linear regression in figure 5 of the measured reflectance versus the predicted reflectance is the degradation coefficient r_1. The intercept and the correlation coefficient are an indicator of the accuracy of the calibration. For 'good' cases, we anticipate an intercept of zero or less than 0·001.

2.3.2. *Error budget*

In the error analysis, we assume that the sensor has a linear response and that the spectral response of the instrument in each channel does not vary with time. The

uncertainties in the calibration include: uncertainties in the radiative computation, as well as errors in input parameters for ozone amount, water vapour amount, ocean colour and pressure, and finally errors in the estimation of I_{12} because of uncertainties in the assumed aerosol type and variability in the wind speed.

Intercalibration coefficient (r_{12}). The error in r_{12} estimated at 1·5 per cent causes a similar error in r_1 (see (15)).

Radiative transfer computation. If the solar zenith angle is smaller than 75°, the accuracy of the radiative transfer calculation based on plane parallel approximation is better than 10^{-3} in reflectance units (Vermote and Tanré 1992). For a normalized radiance level of 0·02 and a solar zenith angle of 75°, the uncertainty is of the order of 1 per cent (see (15)).

Gaseous absorbers. The ozone amount used in the computation, which primarily affects the signal in channel 1, is extracted from the Total Ozone Mapping Spectrometer (TOMS) gridded data (Fishman *et al.* 1990). The assumed absolute accuracy of the ozone amount should be of the order of 20 Dobson units. For an airmass of four, that translates to an uncertainty of 0·6 per cent in the radiance for channel 1, and an uncertainty of 1 per cent in the calibration coefficient (see (15)).

The expected error in total precipitable water vapour is 0·5 g cm^2. An uncertainty in the water vapour amount will translate to an uncertainty in the aerosol correction. The 5S code (Tanré *et al.* 1990) was used to determine the uncertainty on transmission which was found to be $\sim$2 per cent. For a typical clear day with an aerosol optical thickness of 0·1, that translates to a residual reflectance of 2×10^{-4} and an uncertainty of 0·1 per cent in r_1 for a typical value of the numerator of (15).

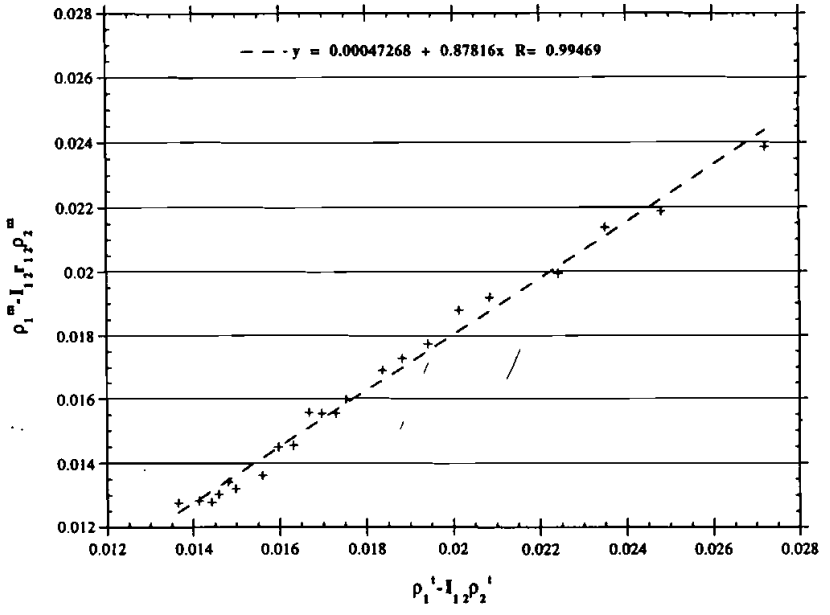

Figure 5. Linear regression between the numerator of (15) (y) and the denominator of (15) (x), that leads to estimate of degradation (r_1) the slope of the linear regression for NOAA-11 on the composite from 2-10 February 1991.

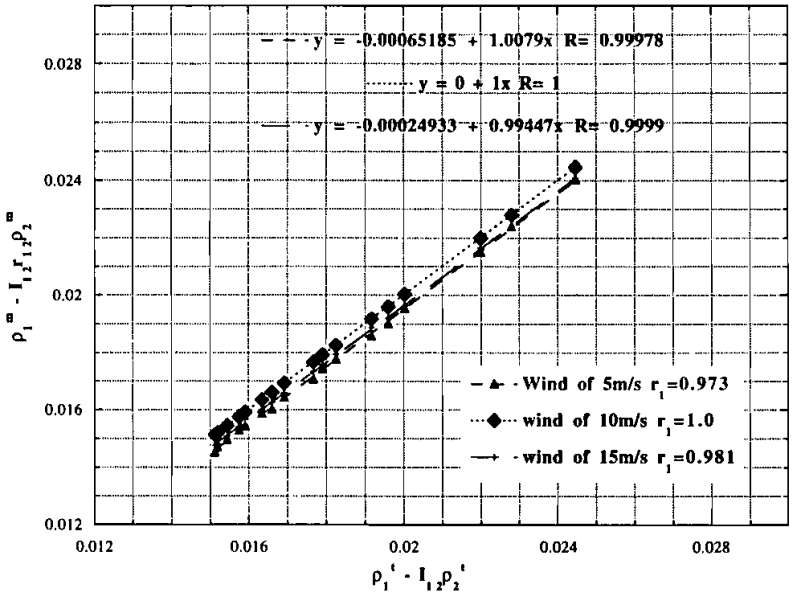

Figure 6. Effect of wind speed on the determination of r_1 ($\Delta r_1 = \pm 0{\cdot}006$).

Ocean colour. The area chosen is over the Pacific Ocean far away from the coast to avoid turbidity in the water. According to Coastal Zone Color Scanner (CZCS) observations the chlorophyll content is lower than $0{\cdot}3\,\mathrm{mg\,m^{-3}}$ and known with an accuracy better than $0{\cdot}1\,\mathrm{mg\,m^{-3}}$. This leads to an uncertainty of 1×10^{-4} in reflectance units for channel 1, which translates to an uncertainty of 0·1 per cent in the calibration coefficient.

Pressure. The area chosen is relatively cloud-free as a result of a high pressure weather system. The pressure used in the computation (1013 mb) is assumed to be known with an accuracy better than 20 mb so that the Rayleigh optical thickness is determined better than 2 per cent in both channels. That leads to an uncertainty of 2 per cent in the calibration coefficient. Once the pressure is known, the Rayleigh optical depth can be computed with an absolute accuracy better than 1 per cent (Teillet 1990).

Wind speed. A simulation was performed to assess the uncertainty induced by wind speed. The wind speed was taken to be $10\,\mathrm{m\,s^{1}}$ and a simulation of the measured radiance was done at $5\,\mathrm{m\,s^{-1}}$ and $15\,\mathrm{m\,s^{-1}}$ with all the other parameters fixed. The wind speed affects the signal at the top of the atmosphere in two ways: over the sun glint by changing the distribution of slopes of the waves (Cox and Munk 1965) and by changing the area covered by foam (Koepke 1984), the latter being the most important effect because the calibration is done in the backscattering direction where the direct sun glint influence is low.

Figure 6 gives the values observed in channels 1 and 2 for the nominal wind speed as well as at $5\,\mathrm{m\,s^{-1}}$ and $15\,\mathrm{m\,s^{1}}$. It also gives the values of the calibration coefficient (equal to 1 for the nominal wind speed). It can be deduced that the effect of wind speed introduces a relative uncertainty of about 2 per cent.

Table 3. Error budget for the absolute calibration of channel 1 using Rayleigh scattering.

Error source	Uncertainty	$\delta r_1/r1$
$\delta r_{12}/r_{12}$	1·2%	1·5%
Radiative transfer code	10^{-3} (reflectance)	1%
Ozone amount	20 Dobson units	1%
Chlorophyll content	$\pm 0{\cdot}1\,\mathrm{mg\,m^{-3}}$	0·1%
Pressure	$\pm 20\,\mathrm{mb}$	2%
Wind speed	$5\text{–}15\,\mathrm{m\,s^{-1}}$	2%
Aerosol		—
Total (r.m.s.)		3·5%

Aerosol type. A simulation was performed for two aerosol types other than the maritime model, used here. For continental aerosol at an optical thickness of 0·1 and 0·25 and for stratospheric aerosol (King *et al.* 1984) at optical thicknesses of 0·1, 0·2 and 0·3. In each case, the error is significant, ranging from 5 per cent (continental) to 15 per cent (stratospheric). We expect that over the Pacific Ocean the presence of continental aerosol will be rare and should be eliminated by the compositing process. Continental aerosol could cause large errors and therefore spikes in the calibration. There are no indications of such spikes in the time series (figure 8), which confirms that there is no contamination by continental aerosol. In cases of significant concentration of stratospheric aerosol, such as after volcanic eruptions of Mount Pinatubo or El Chichon, the method presented is not expected to work, at least not in its current state. Because the model used, Haze M, may be different than the actual aerosol background over the Pacific Ocean we adopt a 3 per cent uncertainty based on the fact that we obtained a 5 per cent error using a continental model.

Total error. The theoretical error budget (table 3) shows that under moderate aerosol loading an overall error of 5 per cent is expected. We expect to filter any dubious results (e.g., due to high aerosol concentration) by the inspection of coefficient of correlation and intercept of the regression. The dispersion of the result over a month (four results) should also confirm our estimate of the error.

3. Results

Figure 7 shows the estimate of the intercalibration coefficient, r_{12} using the cloud technique for NOAA-7, -9 and -11. The dispersion of the results is very low (less than 2 per cent), which confirms that the random errors in the calibration, due to variation in water vapour and aerosol properties, are as small as predicted in the error analysis.

Figure 8 shows the estimate of the degradation in channel 1 based on the ocean technique. The results show high stability (4–5 per cent) of the derived coefficient which is inside the estimated error budget. For NOAA-11, the eruption of Mount Pinatubo has produced, as expected, a large variability. We can filter out these results by inspection of the intercept of the regression and by choice of an alternate zone not contaminated by stratospheric aerosol.

Figure 9 (*a*) shows a comparison for r_{12} between ER-2 calibration method using White Sands views (Smith *et al.* 1988) and the present results using clouds for

NOAA-9. Figure 9(*b*) shows the same comparison for NOAA-11 (Abel *et al.* 1993). Both methods show a similar trend in time. The calibration ratio in the present results is 5-9 per cent higher than those of Abel *et al.* for NOAA-9 and 12-15 per cent for NOAA-11. Also shown is a compilation of other methods by Che and Price (1992). In order to get an independent check on those results, we applied the glint inter-calibration method (Kaufman and Holben 1993). We used channel 3 in order to get an independent assessment of the wind speed, the split window technique to derive the water vapour amount, and a constant aerosol thickness of 0·1 with a maritime aerosol type. The error budget of this method is presented in table 5 and the detailed conditions for the five comparison points in table 4. The error budget shows that the method is less accurate than the cloud method (±4 per cent) but should be of sufficient accuracy to outline if there is an unforeseen problem with the cloud method, especially in the case of NOAA-11. The results obtained compare very well to the cloud results within the error bars of both methods. One of the conclusions is that the ratio reported by Abel *et al.* and others for NOAA-11 is below the ratio derived here by the two independent methods. According to our analysis, the increase in r_{12} between the end of use of NOAA-9 ($r_{12}=1{\cdot}03$) and the first months of use of NOAA-11 ($r_{12}=1{\cdot}21$) is $1{\cdot}17=1{\cdot}21/1{\cdot}03$. This rate of increase in r_{12} is very close to the value computed from the Kaufman and Holben (1993) study: $1{\cdot}16=1{\cdot}16/1{\cdot}0$ but far from the one derived from the Abel (1993) and Smith (1988) results: $1{\cdot}09=1{\cdot}04/0{\cdot}95$. Therefore, we suspect a problem with the Abel and Smith calibration coefficients, probably due to water vapour absorption effect in channel 2.

For the ocean method, figures 10(*a*)-(*b*) show comparison both for NOAA-9 and NOAA-11 between ER-2 calibration and the present results. In both cases, the

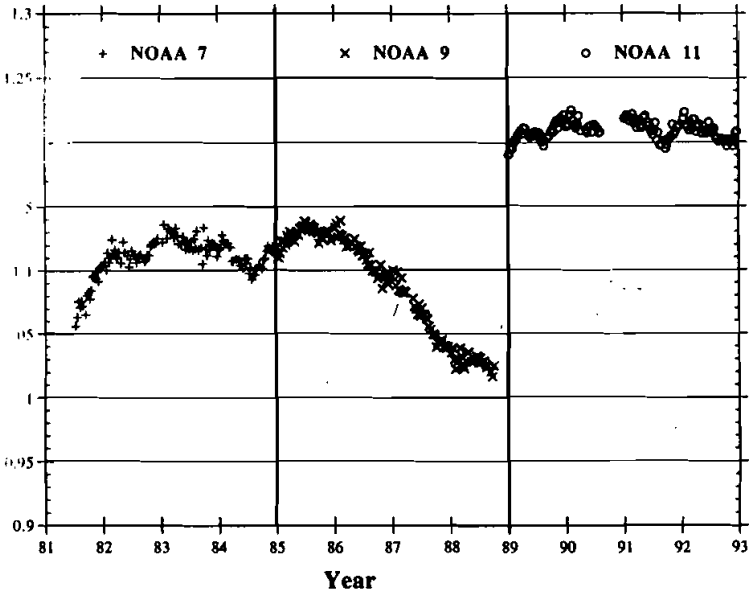

Ratio between the deterioration of channels 1 and 2, r_{12} as observed over high reflective clouds for NOAA-7, -9, -11.

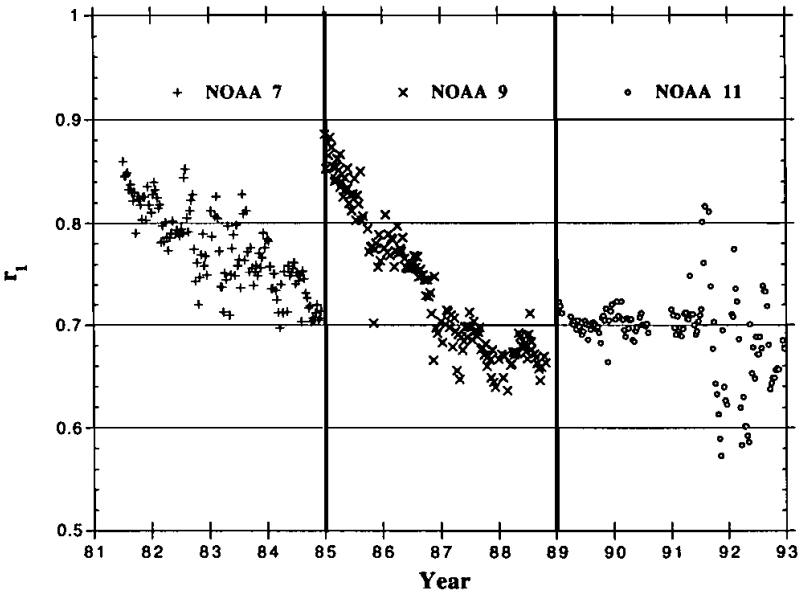

Figure 8. Deterioration of channel 1 of AVHRR as observed using ocean target and the method described in §2.3 for NOAA-7, -9, -11 (e.g., a value of $r_1 = 0{\cdot}8$ means that the sensor is 20 per cent less sensitive than pre-flight).

sensor degradation observed over the ocean is larger than the value determined by the ER-2 or by Che and Price. The estimate for the errors in the present method and in the calibration of Abel *et al.* (1993) or Smith *et al.* (1988) cannot explain, in our opinion, the differences observed in figures 10(*a*)-(*b*). Therefore the differences should be related to the different sensor responses to ocean views, from that of White Sands as in the case of the ER-2 flights. An independent calibration over the oceans was done by Mitchell *et al.* (1992) for NOAA-11, using measurements of aerosol optical thicknesses at Cape Grim. They determined the degradation of both channels of NOAA-11 on 3 April 1990 (see figure 10(*b*)). The r.m.s. sum of the different errors lead to uncertainties of $\pm 0{\cdot}04$ in r_1 and $\pm 0{\cdot}06$ in r_2 (Mitchell *et al.* 1992). They anticipated a small error in the calibration by using measured aerosol optical thicknesses and checking the modelled scattering phase function by using two consecutive satellite overpasses. It is interesting to compare their calibration results to the present one and to those of ER-2. Results of the calibration of Mitchell *et al.* (1992) is within 5 per cent of the present calibration and 10 per cent lower than the ER-2 calibration.

In order to understand the reasons for the differences between the two calibration techniques using radiances over the ocean (the present calibration and that of Mitchell *et al.* (1992)) and the calibration with the ER-2 over the White Sands we test the application of the calibrations to the retrieval of optical thickness from the NOAA-9 AVHRR data over Tasmania, Australia. During January and February 1988, simultaneous ground based measurements of the optical thickness were performed in the Cape Grim observatory (CSIRO 1990) as part of the Baseline Atmospheric program, and supplied to us for individual days by B. Forgan (personal communication 1992). These careful ground based measurements are

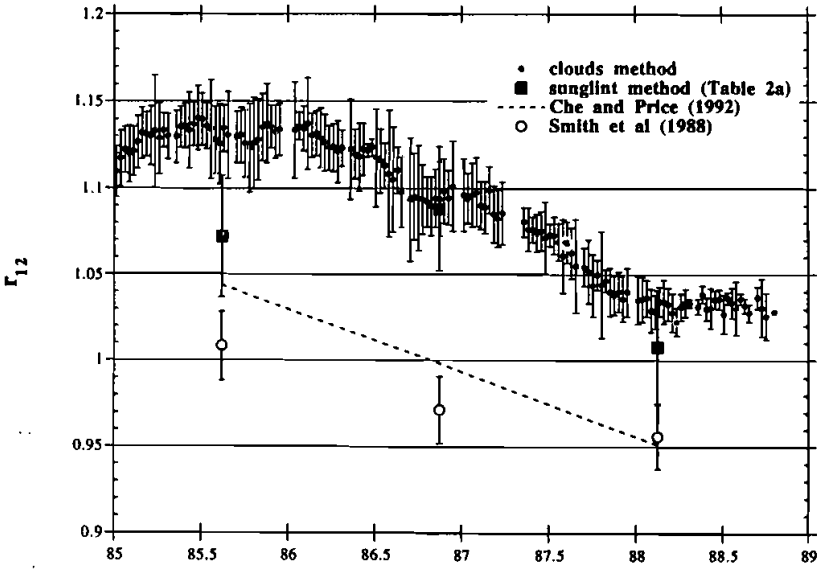

(*a*)

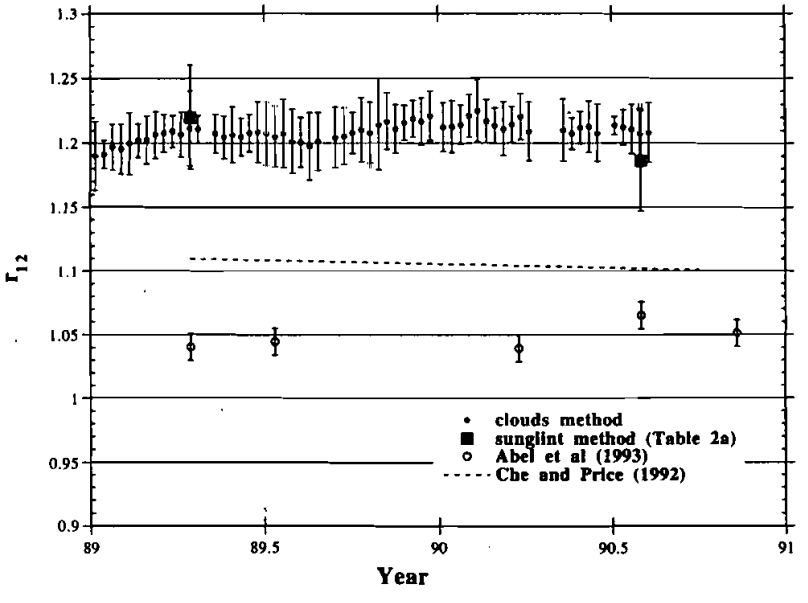

(*b*)

Figure 9. Comparison of r_1/r_2 derived using clouds and other methods. (*a*) NOAA-9; (*b*) NOAA-11.

Table 4. Derivation of the intercalibration between channel 1 and channel 2 (r_1/r_2). based on sun glint observation.

	5/5/1988	6/11/1986	16/8/1985	5/5/1989	10/9/1990
Latitude [°]	7·8	−5·64	30	10·5	−1·5
θ_s	45·3	42·6	28·8	22·7	34·9
θ_v	43·3	46·6	29·5	21·0	17·6
ϕ_s	273·3	254	246	286·1	290·4
ϕ_v	77·8	81·6	77·8	80·3	81·3
ρ_1^m (model)	0·181	0·286	0·199	0·092	0·065
ρ_2^m (model)	0·161	0·253	0·168	0·073	0·048
ρ_1^t (measured)	0·1395	0·262	0·174	0·0813	0·05686
ρ_2^t (measured)	0·12314	0·213	0·137	0·0528	0·0354
Water vapour ($g\,cm^{-2}$)	2	3·6	5	4	3·5
Ozone ($cm\,atm^{-1}$)	0·27	0·26	0·307	0·28	0·28
Wind speed ($m\,s^{-1}$)	7	7	5	10	15
ρ_2^m/ρ_1^m	0·8895	0·8846	0·8442	0·7935	0·7385
ρ_2^t/ρ_1^t	0·8827	0·8130	0·7874	0·6495	0·6226
ρ_1/ρ_2	1·008	1·088	1·072	1·222	1·186

compared to the retrieved optical thicknesses from the satellite data. The results, summarized in Table 6, indicated several problems in the comparison:

(*a*) *Test of the ER-2 calibration*—Aerosol optical thicknesses derived using the ER-2 calibration and a look-up table approach underestimates the optical thickness in channel 1, resulting even in several negative optical thicknesses. This means that the AVHRR measured radiances derived using the ER-2 calibration over the ocean in channel 1 are significantly lower than expected.

(*b*) *Test of the present calibration*—Application of the calibration derived in the present study to the same AVHRR data shows that the derived aerosol optical thicknesses are significantly larger than the optical thickness measured from the ground in both channels.

Several hypothetical reasons or combinations of them can cause the differences between the calibration coefficients derived by the ocean and White Sands methods and between the optical thickness derived by using these calibration coefficients and

Table 5. Error budget for the glint intercalibration method.

Error source	Uncertainty	$\delta r_{12}/r_{12}$
Ozone amount	20 Dobson units	1%
Water vapour	$\pm 0{\cdot}5\,g\,cm^{-2}$	2%
Wind speed	$\pm 2\,m\,s^{-1}$	1%
Optical depth aerosol	±0·1	2%
Aerosol type	Maritime-continental	1%
Total (r.m.s.)		3·3%

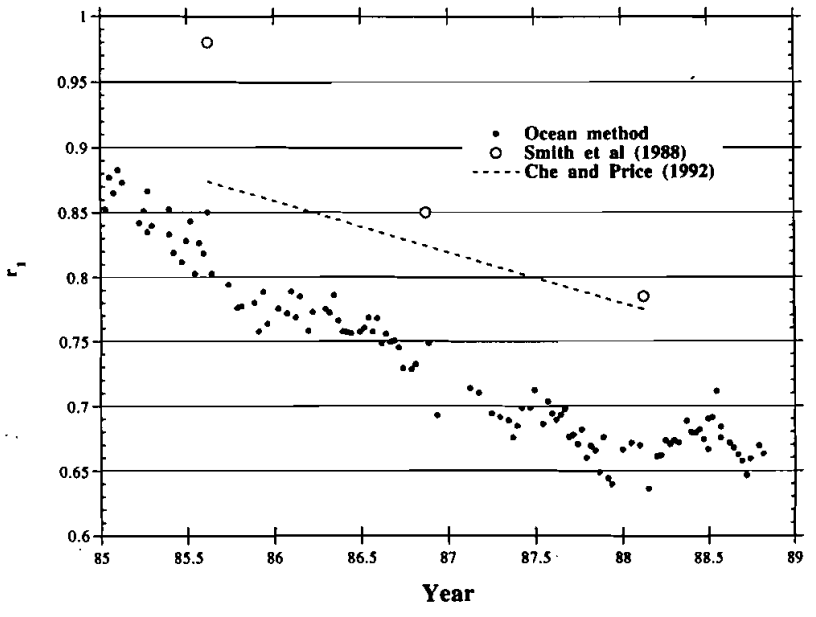

(*a*)

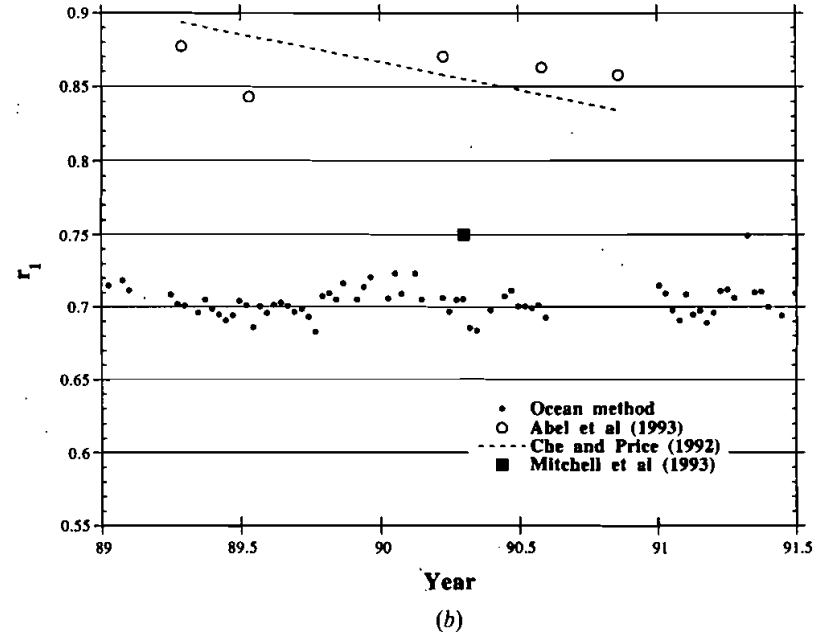

(*b*)

Figure 10. Comparison of the r_1 derived using ocean and other methods. (*a*) NOAA-9; (*b*) NOAA-11.

Table 6. Analysis of the optical depth values recorded over the coast of Tasmania during 1988 with those derived from NOAA-9 using several calibration hypotheses: (1) ER-2 calibration; (2) Present studies; (3) ER-2 calibration with a shift of 17 nm toward the red of channel 1 effective wavelength.

Julian Day	τ 0·5 μm	τ 0·86 μm	$\tau_{ch1(1)}$ $r_1=0{\cdot}78$	$\tau_{ch2(1)}$ $r_1=0{\cdot}82$	$\tau_{ch1(2)}$ $r_1=0{\cdot}62$	$\tau_{ch2(2)}$ $r_1=0{\cdot}62$	$\tau_{ch1(3)}$ $r_1=0{\cdot}78$
19	0·04	0·04	0·0	0·05	0·09	0·10	0·05
28	0·02	0·03	−0·01	0·03	0·07	0·07	0·04
31	0·10	0·09	0·06	0·12	0·15	0·18	0·10
40	0·07	0·07	−0·02	0·03	0·05	0·07	0·02
46	0·055	0·055	0·02	0·06	0·10	0·11	0·06
47	0·02	0·02	−0·03	0·02	0·05	0·06	0·02
48	0·03	0·03	−0·05	0·03	0·04	0·07	0·01
55	0·03	0·03	−0·03	0·02	0·05	0·06	0·02
57	0·06	0·06	0·05	0·11	0·16	0·17	0·11
58	0·04	0·04	0·03	0·11	0·13	0·16	0·08
65	0·03	0·03	0·01	0·06	0·11	0·11	0·06
66	0·035	0·04	−0·03	0·04	0·06	0·09	0·02
76	0·05	0·05	0·02	0·08	0·12	0·14	0·08
77	0·05	0·05	0·03	0·06	0·11	0·10	0·07
Mean	0·042	0·045	0·0005	0·059	0·09	0·11	0·053

the ground truth. We ruled out the possibility of a nonlinear gain of the AVHRR, since the regression lines to the present calibration data are linear, the analysis of AVHRR data over targets with different reflectances by Brest and Rossow (1992) showed linearity and the intrinsic structure of the sensor with silicon detector makes nonlinearity virtually impossible. Polarization sensitivity could not explain the difference. In the case of the present study, the data used are close to the backscattering direction, in this case the Rayleigh scattering does not polarize enough to explain the higher degradation observed even with a 100 per cent polarization sensitivity. Such sensitivity would produce over sea some characteristic geometrical features that are not observed. A change in the filter response by outgazing would produce a shift to shorter wavelength (Dinguirard 1993, personal communication). Mekler and Kaufman (1995), simulated in laboratory the outgazing/aging effect for the AVHRR filters and did not find any significant change in the response.

The only single phenomenon that can explain, simultaneously, *all* the discrepancies described here is a possible shift in the *effective* wavelength of channel 1 to a longer wavelength by 17 nm. This shift would reduce the Rayleigh optical thickness from 0·058 to 0·052. This smaller Rayleigh optical thickness will affect the present calibration using oceans and affect retrieval of aerosol optical thicknesses over Tasmania using any of these calibrations. A similar shift in channel 2 could not be detected due to the small Rayleigh optical thickness in this channel. More specifically the following changes are anticipated from the smaller Rayleigh optical thickness:

(*a*) A larger aerosol optical thickness in channel 1 derived from the AVHRR data using the White Sands calibration of Abel *et al.* (1993). Table 6 shows a good fit between the newly retrieved aerosol optical thicknesses and the ground truth (last column).

(*b*) The reduction in the Rayleigh optical thickness causes a decrease in model radiances and a smaller degradation of the sensor in the present calibration method. Figures 11 (*a*)-(*b*) compare the newer calibration using the present method with that of the ER-2 calibration. The agreement is much better for both NOAA-9 and -11 and within the stated accuracy.

(*c*) The lower Rayleigh optical thickness will also affect the calibration of Mitchell *et al.* (1992). They reported aerosol optical depth of $0{\cdot}3 \pm 0{\cdot}01$, and Rayleigh contribution of 83 per cent (see table 5 of Mitchell *et al.* 1992). Considering a shift of 17 nm, the Rayleigh optical thickness will decrease by 11·5 per cent, causing the calibration coefficient to increase by 9·6 per cent. The 'revised' calibration coefficient of 0·82, plotted in figure 11 (*b*) shows also a good agreement with ER-2 results and the results from the present study.

(*d*) The revised calibration in the present method was used to derive the aerosol optical thickness over Tasmania and shown in table 6. The new results are similar to the ground based measurements in both channels!

We showed that a hypothetical shift of 17 nm occurring immediately after launch, both for NOAA-9 and -11 can explain several discrepancies between the three calibration methods and between the aerosol optical thickness over Tasmania derived using these calibrations and the ground based measurements.

This shift in the *effective* wavelength does not necessarily mean a shift of the whole spectral channel. Lower transmission in the shorter wavelength part of the channel can also translate to an effective shift.

Two effects that occur immediately after launch can cause a change in the calibration and a shift in the spectral response: a disalignment of optics or deposit on the optics of small particles from the burning fuel (Mekler and Kaufman 1995). Such deposits were detected in the NASA LDEF experiment as a brown film of hydrocarbons deposited on the optical surfaces exposed to space (Harvey 1991). Measurements of the transmission curves of the deposit shows that the deposit absorbs strongly in the UV, with transmission increasing from 0 at 0·2 μm to 60 per cent at 0·38 μm. No measurements were reported in the visible part of the spectrum. If this spectral absorption continues into the visible part of the spectrum, then it can cause a shift in the effective wavelength of the AVHRR channel 1.

4. Conclusions

A new method for absolute calibration for the visible and near-infrared channels of the AVHRR was presented. It is based on a combination of observations over remote ocean areas and over high reflective clouds located in the tropics over the Pacific Ocean. Clouds are used to find the ratio between the calibration of channels 1 and 2, assuming that the reflectance of cloud drops is spectrally neutral, and locating a temperature range for which the high reflective clouds are not affected by water vapour absorption and radiation field under the cloud. Calibration over oceans is based on the large contribution of molecular scattering in the atmosphere over the oceans, and elimination of the uncertain aerosol contribution using a combination of radiances in channel 1 and 2. In essence, after the cloud intercalibration between the two channels, channel 2 is used to subtract the aerosol effect from the radiance in channel 1. While previous applications of a similar technique to SPOT and GOES data resulted in a calibration that agreed very well with independent information, application for the AVHRR on NOAA-7, -9 and -11 resulted in calibration that is

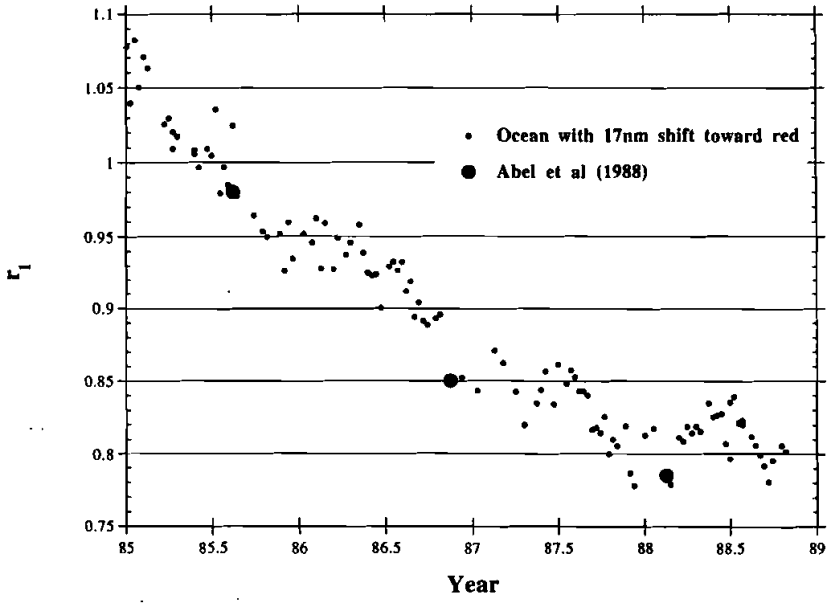

(*a*)

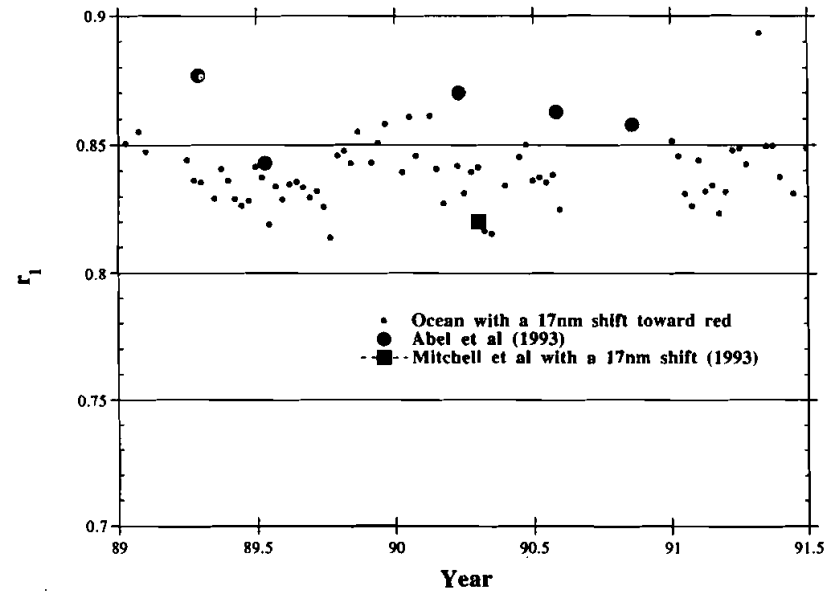

(*b*)

Figure 11. Same as figure 9 but with the assumption of a shift of 17 nm of the central wavelength of channel 1 toward the red. (*a*) NOAA-9; (*b*) NOAA-11.

much different from the expected values from ER-2 calibration over White Sands. The trend of the calibration derived by the present method is very similar to the White Sands calibration and calibrations over deserts. The present method resulted in a very stable calibration, that is derived continuously with time.

Error analysis, supported by the low noise in the calibration, shows that the method should give the absolute calibration within 5 per cent. The success of application to SPOT and GOES satellite systems, and the prediction of small errors leads us to believe that the difference between the present AVHRR calibration and that over White Sands is not due to flaws in the calibration methods.

We compared the application of these two calibration methods to derive the aerosol optical thickness over Tasmania, where ground based measurements are available. Both the present method and the ER-2-White Sands method *failed to predict* correctly the optical thickness. The only process that we found to explain simultaneously the differences in the calibrations and the errors in remote sensing of aerosol optical thickness for NOAA-9 and -11 is a spectral shift of the AVHRR channel 1 effective wavelength by 17 nm towards longer wavelengths. One possible explanation of such a shift is a contamination of the AVHRR exposed external mirror to rocket exhaust during launch that may reduce its sensitivity to shorter wavelength. Such contamination was found in the LDEF experiment. Recent work in preparation for publication (Vermote *et al.*, 1995, in preparation) indicates that this shift is due to an out of band transmission (6 per cent at 900 nm) for AVHRR channel 1 previously unidentified.

The method can be applied to other satellite systems, e.g., the SeaWiFS planned to be launched in 1994, to find the absolute calibration as was done for GOES and SPOT or to test the spectral response as in the present case. We expect the method to work better for SeaWiFS because the availability of short wavelength channels (450 nm), can reduce the errors in the absolute calibration to 3 per cent.

Acknowledgments

The authors would like to thank Bruce Forgan for kindly providing aerosol measurements over Cape Grim, Nazmi El Saleous for having written the AVHRR data processing software used in this study and George Vasilliou for his help in the early part of the project.

References

ABEL, P., GUENTHER, B., GALIMORE, R. N., and COOPER, J. W., 1993, Calibration results for NOAA-11 AVHRR channels 1 and 2 from congruent path aircraft observations. *Journal of Atmospheric and Oceanic Technology*, **10**, 493-508.

ARKING, A., and CHILDS, J. D., 1985, Retrieval of cloud cover parameters from multispectral satellite images. *Journal of Climate and Applied Meteorology*, **24**, 322-333.

BREST, C. L., and ROSSOW, W. L., 1992, Radiometric calibration and monitoring of NOAA AVHRR data for ISCCP. *International Journal of Remote Sensing*, **13**, 235-273.

CHE, N., and PRICE, J. C., 1992, Survey of radiometric calibration results and methods for visible and near infrared channels of NOAA-7, -9, and -11 AVHRRs. *Remote Sensing of Environment*, **41**, 19-27.

COAKLEY, R., BERNSTEIN, L., and DURKEE, P. A., 1987, Effect of ship stack effluents on cloud reflectance. *Science*, **237**, 953-1084.

COX, C., and MUNK, W., 1965, Slopes of the sea surface deduced from photographs of sun glitter. *Bulletin of Scripps Institute of Oceanography of University of California*, **6**, 401-488.

DALU, G., 1986, Satellite remote sensing of atmospheric water vapour. *International Journal of Remote Sensing*, **7**, 1089–1097.

DEUZÉ, J. L., HERMAN, M., and SANTER, R., 1989, Fourier series expansion of the transfer equation in the atmosphere-ocean system. *Journal of Quantitative Spectroscopy and Radiative Transfer*, **41**, 483–494.

FISHMAN, J., WATSON, C. E., LARSEN, J. C., and LOGAN, J. A., 1990, Distribution of tropospheric ozone determined from satellite data. *Journal of Geophysical Research*, **95**, 3599–3617.

FORGAN, B. W., and FRASER, P. J., 1987, Baseline atmospheric program (Australia) 1985, Department of Science, Cape Grim, Australia.

FRASER, R. S., and KAUFMAN, Y. J., 1986, Calibration of satellite sensors after launch. *Applied Optics*, **25**, 1177–1185.

FRASER, R. S., FERRARE, R. A., KAUFMAN, Y. J., MARKHAM, B. L., and MATTOO, S., 1992, Algorithm for atmospheric corrections of aircraft and satellite imagery. *International Journal of Remote Sensing*, **13**, 541–557.

FROUIN, R., and GAUTIER, C., 1987, Calibration of NOAA-7 AVHRR, GOES-5 and GOES-6 VISSR/VAS solar channels. *Remote Sensing of Environment*, **22**, 73–101.

HARVEY, G. A., 1991, Effects of long duration exposure on optical system components. *Proceedings First Post-Retrieval Symposium*, edited by A. S. Levine, NASA Conference Publication 3134 (Washington, D.C.: NASA), pp. 1327–1340.

HOLBEN, B. N., 1986, Characteristics of maximum-value composite images from temporal AVHRR data. *International Journal of Remote Sensing*, **7**, 1417–1434.

HOLBEN, B. N., KAUFMAN, Y. J., and KENDALL, J. D., 1990, NOAA-11 AVHRR visible and near-IR inflight calibration. *International Journal of Remote Sensing*, **11**, 1511–1519.

HOLBEN, B. N., VERMOTE, E., KAUFMAN, Y. J., TANRÉ, D., and KALB, V., 1992, Aerosols retrieval over land from AVHRR data—application for atmospheric correction. *I.E.E.E. Transactions on Geoscience and Remote Sensing*, **30**, 212–222.

JUSTICE, C. O., TOWNSHED, J. R. G., HOLBEN, B. N., and TUCKER, C. J., 1985, Analysis of the phenology of global vegetation using meteorological satellite data. *International Journal of Remote Sensing*, **6**, 1271–1318.

KAUFMAN, Y. J., and HOLBEN, B. N., 1993, Calibration of the AVHRR visible and near-IR bands by atmospheric scattering, ocean glint and desert reflection. *International Journal of Remote Sensing*, **14**, 21–52.

KAUFMAN, Y. J., and NAKAJIMA, T., 1993, 'Effect of Amazon smoke on cloud microphysics and albedo'. *Journal of Applied Meteorology, Squires special issue*, **32**, 729–744.

KAUFMAN, Y. J., FRASER, R. S., and FERRARE, R. A., 1990, Satellite remote sensing of large scale air pollution-method. *Journal of Geophysical Research*, **95**, 9895–9909.

KING, M., HARSHVARDHAN, D., and ARKING, A., 1984, A model of the radiative properties of the El Chichon stratospheric aerosol layer. *Journal of Climate and Applied Meteorology*, **23**, 1121–1137.

KOEPKE, P., 1982, Vicarious satellite calibration in the solar spectral range by means of calculated radiances and its application to Meteosat. *Applied Optics*, **21**, 2845–2854.

KOEPKE, P., 1984, Effective reflectance of oceanic white caps. *Applied Optics*, **23**, 1816–1824.

MCCORMICK, M. P., and VEIGA, R. E., 1992, SAGE II measurements of early Pinatubo aerosols. *Geophysical Research Letters*, **19**, 155–158.

MEKLER, YU. and KAUFMAN, Y. J., 1995, On possible causes of calibration degradation of the AVHRR visible and near IR channels. *Applied Optics*, **34**, 1059–1062.

MITCHELL, R. M., O'BRIEN, D. M., and FORGAN, B. W., 1992, Calibration of the NOAA AVHRR shortwave channels using split pass imagery: I. Pilot study. *Remote Sensing of Environment*, **40**, 57–65.

MOREL, A., 1988, Optical modeling of the upper ocean in relation to its biogenous matter content (case I waters). *Journal of Geophysical Research*, **93**, 10479–10768.

PRICE, J. C., 1987, Calibration of satellite radiometers and the comparison of vegetation indexes. *Remote Sensing of Environment*, **21**, 15–27.

PRICE, J. C., 1988, An update on visible and near IR calibration of satellite instruments. *Remote Sensing of Environment*, **24**, 419–422.

RAO, C. R., CHEN, J., STAYLOR, F. W., ABEL, P., KAUFMAN, Y. J., VERMOTE, E., ROSSOW, W. R., and BREST, C., 1993, Degradation of the visible and near IR channels of the

AVHRR on the NOAA-9 spacecraft: assessment and recommendations for corrections, NOAA Technical Report NESDIS 70 (National Oceanic and Atmospheric Administration, Washington, D.C.).

SMITH, G. R., LEVIN, R. H., ABEL, P., and JACOBOWITZ, H., 1988, Calibration of the solar channels of the NOAA-9 AVHRR using high altitude aircraft measurements. *Journal of Atmospheric and Oceanic Technology*, **5**, 631-639.

STAYLOR, W. F., 1990, Degradation rates of the AVHRR visible channel for the NOAA 6, 7 and 9 spacecraft. *Journal of Atmospheric and Oceanic Technology*, **7**, 411-423.

STOWE, L. L., MCCLAIN, E. P., CAREY, R., PELLEGRINO, P., GUTMAN, G. G., DAVIS, P., LONG, C., and HART, S., 1991, Global distribution of cloud cover derived from NOAA/AVHRR operational satellite data. *Advances in Space Research*, **11**, 51-54.

STOWE, L. L., CAREY, R. M., and PELLEGRINO, P. P., 1992, Monitoring the Mt. Pinatubo aerosol layer with NOAA/11 AVHRR data. *Geophysical Research Letters*, **19**, 159-162.

TANRÉ, D., DEROO, C., DUHAUT, P., HERMAN, M., MORCETTE, J. J., PERBOS, J., and DESCHAMPS, P. Y., 1990, Description of a computer code to simulate the satellite signal in the solar spectrum: 5S code. *International Journal of Remote Sensing*, **11**, 659-668.

TEILLET, P. M., 1990, Rayleigh optical depth comparisons from various sources. *Applied Optics*, **29**, 1897-1990.

TEILLET, P. M., SLATER, P. N., DING, Y., SANTER, R. P., JACKSON, R. D., and MORAN, M. S., 1990, Three methods for the absolute calibration of the NOAA AVHRR sensors in-flight. *Remote Sensing of Environment*, **31**, 105-120.

TUCKER, C. J., and SELLERS, P. J., 1985, Satellite remote sensing of primary production. *International Journal of Remote Sensing*, **7**, 1395-1416.

VERMOTE, E. R., and TANRÉ, D., 1992, Analytical expressions for radiative properties of planar Rayleigh scattering media including polarization contribution. *Journal of Quantitative Spectroscopy and Radiative Transfer*, **47**, 305-314.

VERMOTE, E., SANTER, R., DESCHAMPS, P. Y., and HERMAN, M., 1992, In-flight calibration of large field of view sensors at short wavelengths using Rayleigh scattering. *International Journal of Remote Sensing*, **13**, 3409-3429.

VERMOTE, E., EL SALEOUS, N., and HOLBEN, B. N., 1993, Atmospheric correction of the AVHRR visible and near infrared data. *Proceedings of the Workshop on Atmospheric Correction of Landsat Data, held in Torrance, California, on 29 June–1 July 1993*, (Torrance, California: Geodynamics Corporation).